International Journal of Solids and Structures 90 (2016) 1–11

Contents lists available at ScienceDirect

International Journal of Solids and Structures

journal homepage: www.elsevier.com/locate/ijsolstr

Surface cracking in an orthotropic medium subjected to frictional contact

Duygu Sarikaya, Serkan Dag*

Department of Mechanical Engineering, Middle East Technical University, Ankara 06800, Turkey

ARTICLE INFO

Article history:
Received 17 December 2015
Revised 22 February 2016
Available online 19 April 2016

Keywords:
Orthotropic materials
Contact mechanics
Fracture mechanics
Surface crack
Singular integral equations

ABSTRACT

This article presents an analytical method capable of resolving the coupled problem of surface cracking in an orthotropic elastic medium subjected to frictional contact by a rigid flat punch. Reciprocal influences between the surface crack and the flat punch are accounted for by establishing a fully coupled formulation. Governing partial differential equations involving the displacement components are derived in accordance with plane theory of orthotropic elasticity. General solutions corresponding to mode I and II crack problems and contact problem are obtained employing Fourier transformation techniques. These separate solutions are then reconciled; and three coupled singular integral equations are developed by applying crack surface and contact zone conditions. Singular integral equations are solved numerically through an expansion–collocation method in which the primary unknowns are expanded into series in terms of Jacobi polynomials. Comparisons to the results available in the literature for certain special cases do verify the proposed procedures. Further numerical results are presented to be able to demonstrate the influences of material orthotropy, coefficient of friction, and geometric parameters upon the mixed-mode stress intensity factors and the contact stress.

1. Introduction

Quite a large number of engineering materials utilized in technological applications possess an orthotropic macro-structure. Orthotropy is a reduced type of general anisotropy, which stems from the existence of two orthogonal planes of elastic symmetry within a medium. It is encountered not only in conventional composites like fiber reinforced plates and shells but also in newer material systems such as thin films and coatings. Orthotropy in thin films is a result of the processing method. For instance, electron beam physical vapor deposition induces a columnar thin film structure whereas plasma spray technique causes a lamellar type formation. Because of the importance and common usage of orthotropic materials in both conventional and arising fields of technology, there is a vast amount of literature on related mechanics problems, particularly on contact and fracture mechanics.

Solutions in literature on contact mechanics of orthotropic materials depict a clear picture of the influences of material properties and loading parameters on stress distributions. Certain fundamental findings on contact mechanics of anisotropic half-planes are compiled in the book by Kachanov et al. (2003). More recent advances in contact mechanics of orthotropic media include developments pertaining to indentation (Shi et al., 2003), Hertzian contact (Swanson, 2004), frictional moving punch problems (Zhou et al., 2014), and contact with collinear stamps (Dong et al., 2014). Results on fracture mechanics of orthotropic materials are essential to quantify critical and sub-critical crack propagation phenomena. For this reason, stress intensity factors (SIFs) are computed for a variety of crack configurations. Newer results regarding such research work are generated for multiple interacting cracks (Baghestani et al., 2013), an edge cracked orthotropic strip (Matbuly and Nassar, 2003), a dynamically loaded cracked half-plane (Monfared and Ayatollahi, 2012), an inclined crack in an infinite medium (Nobile et al., 2004), and thermally loaded collinear cracks (Zhong et al., 2013).

Certain types of cracking failures in engineering materials require simultaneous consideration of fracture and contact problems. This is especially the case for brittle materials under the effect of severe contact loadings. Primary cracking mechanisms in the vicinity of contact zones in such materials are: Radial cracking due to Vickers indentation (Page and Knight, 1989), Hertzian cracking due to loading by a blunt indenter (Lawn, 1995), and herringbone cracking due to sliding frictional contact (Suresh et al., 1999). Moreover, surfaces subjected to oscillating frictional forces tend to develop fretting fatigue cracks (Nesladek et al., 2012; Hills and Nowell, 2014). Studies on the behavior of cracks located in the

* Corresponding author. Tel.: +90 312 2102580; fax: +90 312 2102536.
E-mail address: sdag@metu.edu.tr (S. Dag).

http://dx.doi.org/10.1016/j.ijsolstr.2016.04.018
0020-7683/

vicinity of a contact zone are required to understand these failure mechanisms. Analytical research work has been undertaken to examine fracture in isotropic homogeneous and functionally graded materials caused by sliding frictional contact (Hasebe et al., 1989; Hasebe and Qian, 1998; Dag, 2001; Dag and Erdogan, 2002). However, there has been no prior work on such problems in orthotropic materials.

Formulation of the problem of cracking due to sliding contact for orthotropic materials is substantially different from those developed for isotropic homogeneous and functionally graded materials. Constitutive relations of orthotropic materials contain four elastic constants in the case of plane stress, and seven in the case of plane strain. Two elastic constants and an inhomogeneity parameter are needed for FGMs; whereas for the isotropic homogeneous case specification of two elastic constants suffices. Distinct structure of the constitutive law leads to a different set of partial differential equations for orthotropic materials. Application of Fourier transform techniques then results in completely different general solutions, which depend on the elastic constants of orthotropy. As a consequence, the terms and kernels of the singular integral equations are not same as those found for isotropic homogeneous or functionally graded materials. For this reason, all formulation steps need to be reapplied for orthotropic materials; and general solutions and singular integral equations have to be derived from scratch in terms of engineering constants of plane orthotropy.

The present study puts forward an analytical approach capable of solving the coupled problem of cracking due to sliding contact in an *orthotropic* medium. For this purpose, a surface crack in an orthotropic half-plane in sliding frictional contact with a rigid punch is considered. Governing partial differential equations in terms of the displacement components are derived by employing the elements of plane orthotropic elasticity. Crack and contact problems are formulated separately by means of Fourier transform techniques. Primary unknown functions in these formulations are respectively relative crack surface displacement derivatives and contact stress for the crack and contact problems. These two separate formulations are then reconciled and reduced to a system of three coupled singular integral equations. The integral equations are solved numerically by an expansion–collocation technique, in which primary unknowns are expanded into finite series entailing Jacobi polynomials. Numerical analyses are carried out to compute mode I and II stress intensity factors and contact stress as functions of degree of orthotropy, coefficient of friction, and geometric parameters.

2. Formulation

The coupled problem of surface cracking in an orthotropic medium due to sliding contact is illustrated in Fig. 1. An elastic orthotropic half-plane lies in the region $x_1 > 0$ and $-\infty < x_2 < \infty$. x_1- and x_2-axes are the principal axes of orthotropy. The half-plane contains a crack located at $x_2 = 0$; and is in sliding frictional contact with a rigid flat punch. Contact zone extends from $x_2 = b$ to $x_2 = c$. The elastic medium is assumed to be in a state of either plane stress or plane strain. Normal and friction forces transferred by the contact are respectively designated by P and Q, where $Q = \eta P$, η being the coefficient of friction.

The formulation is based on the constitutive relations of plane orthotropic elasticity, which are expressed as:

$$\begin{bmatrix}\sigma_{11}\\ \sigma_{22}\\ \sigma_{12}\end{bmatrix} = \begin{bmatrix}C_{11} & C_{12} & 0\\ C_{12} & C_{22} & 0\\ 0 & 0 & C_{66}\end{bmatrix}\begin{bmatrix}\varepsilon_{11}\\ \varepsilon_{22}\\ \varepsilon_{12}\end{bmatrix}, \tag{1}$$

where elements of the stiffness matrix are given by

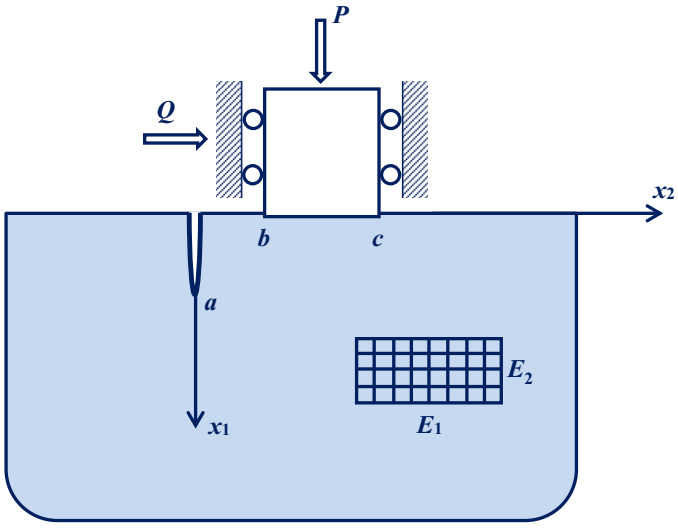

Fig. 1. Geometry of the coupled problem.

$$C_{11} = \begin{cases} \dfrac{E_1}{1-\nu_{12}\nu_{21}}, & \text{for plane stress,}\\ \dfrac{E_1(1-\nu_{23}\nu_{32})}{1-\nu_{12}\nu_{21}-\nu_{13}\nu_{31}-\nu_{23}\nu_{32}-2\nu_{12}\nu_{23}\nu_{31}}, & \text{for plane strain,}\end{cases} \tag{2a}$$

$$C_{12} = \begin{cases} \dfrac{E_2\nu_{12}}{1-\nu_{12}\nu_{21}}, & \text{for plane stress,}\\ \dfrac{E_2(\nu_{12}+\nu_{13}\nu_{32})}{1-\nu_{12}\nu_{21}-\nu_{13}\nu_{31}-\nu_{23}\nu_{32}-2\nu_{12}\nu_{23}\nu_{31}}, & \text{for plane strain,}\end{cases} \tag{2b}$$

$$C_{22} = \begin{cases} \dfrac{E_2}{1-\nu_{12}\nu_{21}}, & \text{for plane stress,}\\ \dfrac{E_2(1-\nu_{13}\nu_{31})}{1-\nu_{12}\nu_{21}-\nu_{13}\nu_{31}-\nu_{23}\nu_{32}-2\nu_{12}\nu_{23}\nu_{31}}, & \text{for plane strain,}\end{cases} \tag{2c}$$

$$C_{66} = 2\mu_{12}, \text{ for both plane stress and strain.} \tag{2d}$$

For an orthotropic material, following inequalities are deduced by considering the fact that strain energy density function is positive definite (Agarwal and Broutman, 1990):

$$1-\nu_{12}\nu_{21} > 0,\ 1-\nu_{13}\nu_{31} > 0,\ 1-\nu_{23}\nu_{32} > 0, \tag{3a}$$

$$1-\nu_{12}\nu_{21}-\nu_{13}\nu_{31}-\nu_{23}\nu_{32}-2\nu_{12}\nu_{23}\nu_{31} > 0. \tag{3b}$$

Governing partial differential equations are derived by using the constitutive relations in conjunction with equilibrium equations and kinematic relations; and expressed as given below:

$$d_{11}\frac{\partial^2 u_1}{\partial x_1^2} + \frac{\partial^2 u_1}{\partial x_2^2} + (1+d_{12})\frac{\partial^2 u_2}{\partial x_1 \partial x_2} = 0, \tag{4a}$$

$$\frac{\partial^2 u_2}{\partial x_1^2} + d_{22}\frac{\partial^2 u_2}{\partial x_2^2} + (1+d_{12})\frac{\partial^2 u_1}{\partial x_1 \partial x_2} = 0, \tag{4b}$$

$$d_{11} = \frac{2C_{11}}{C_{66}}, \quad d_{12} = \frac{2C_{12}}{C_{66}}, \quad d_{22} = \frac{2C_{22}}{C_{66}}. \tag{4c}$$

u_1 and u_2 here are the scalar components of the displacement vector in x_1- and x_2-directions, respectively. The solution has to satisfy

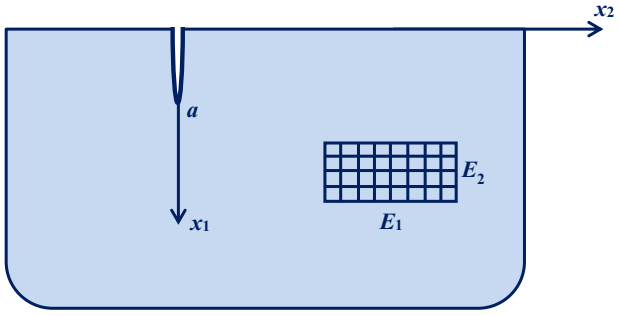

Fig. 2. The mixed-mode crack problem.

the conditions:

$$\sigma_{11}(0,x_2)=\sigma_{12}(0,x_2)=0,\quad x_2<b \text{ and } x_2>c, \tag{5a}$$

$$\sigma_{12}(0,x_2)=\eta\sigma_{11}(0,x_2),\quad b<x_2<c, \tag{5b}$$

$$\sigma_{22}(x_1,0)=\sigma_{12}(x_1,0)=0,\quad 0<x_1<a, \tag{5c}$$

$$\frac{\partial u_1(0,x_2)}{\partial x_2}=0,\quad b<x_2<c, \tag{5d}$$

$$\int_b^c \sigma_{11}(0,x_2)dx_2=-P. \tag{5e}$$

Furthermore, regularity condition requires that all field quantities be bounded as $\sqrt{x_1^2+x_2^2}\to\infty$. Note that Eq. (5c) assumes that there is no contact of the crack faces. However, the results produced through this formulation will still be applicable in the presence of crack closure, provided that they are used as a part of a superposition scheme for a combined loading that leads to a fully open crack.

The first step in our analysis is the development of the general solutions for the crack and contact problems. Crack problem is formulated in terms of the relative displacements of the crack faces whereas contact formulation hinges on the contact stress. These two formulations are then combined to obtain the singular integral equations for the coupled problem. In what follows below, we first elaborate upon the formulations of crack and contact problems.

2.1. Crack problem

Fig. 2 illustrates the geometry of the surface crack problem analyzed in this section. The crack is assumed to be under the effect of mixed-mode loading. Field quantities are derived in terms of the derivatives of relative crack surface displacements. Mode I and II problems are uncoupled in this formulation owing to the symmetry of material distribution and geometry about x_1- axis. Hence, general solutions can be derived by treating mode I and II problems separately.

2.1.1. Mode I problem

The mode I problem is formulated in terms of the derivative of the relative normal crack surface displacement, which is mathematically expressed as

$$f_1(x_1)=\frac{C_{66}}{2}\frac{\partial}{\partial x_1}\left(u_2(x_1,0^+)-u_2(x_1,0^-)\right),0<x_1<a. \tag{6}$$

Boundary and continuity conditions that need to be implemented in the formulation of the mode I problem are:

$$\sigma_{11}(0,x_2)=\sigma_{12}(0,x_2)=0\quad,-\infty<x_2<\infty, \tag{7a}$$

$$\sigma_{22}\left(x_1,0^+\right)=\sigma_{22}\left(x_1,0^-\right),\quad 0<x_1<\infty, \tag{7b}$$

$$\sigma_{12}\left(x_1,0^+\right)=\sigma_{12}\left(x_1,0^-\right),\quad 0<x_1<\infty, \tag{7c}$$

$$u_1\left(x_1,0^+\right)=u_1\left(x_1,0^-\right),\quad 0<x_1<\infty, \tag{7d}$$

$$u_2\left(x_1,0^+\right)=u_2\left(x_1,0^-\right),\quad a<x_1<\infty. \tag{7e}$$

Applying Fourier, Fourier cosine and Fourier sine transforms to the governing partial differential equations, general solutions for the displacement components are derived to be:

$$u_1(x_1,x_2)=\frac{1}{2\pi}\int_{-\infty}^{\infty}\sum_{j=3}^{4}C_j\exp(n_jx_2+i\omega x_1)\,d\omega + \int_0^{\infty}\left(\sum_{j=3}^{4}B_j\exp\left(p_jx_1\right)\right)\cos(\alpha x_2)d\alpha, \quad x_1>0,\quad x_2>0, \tag{8a}$$

$$u_2(x_1,x_2)=\frac{1}{2\pi}\int_{-\infty}^{\infty}\sum_{j=3}^{4}C_jA_j\exp(n_jx_2+i\omega x_1)\,d\omega + \int_0^{\infty}\left(\sum_{j=3}^{4}B_jD_j\exp\left(p_jx_1\right)\right)\sin(\alpha x_2)d\alpha, \quad x_1>0,\quad x_2>0, \tag{8b}$$

where

$$n_3=-E\ |\omega|,\quad n_4=-F\ |\omega|, \tag{9a}$$

$$E=\frac{1}{2}\sqrt{\frac{2}{d_{22}}\left(\beta_1+\sqrt{\beta_2}\right)},\quad F=\frac{1}{2}\sqrt{\frac{2}{d_{22}}\left(\beta_1-\sqrt{\beta_2}\right)}, \tag{9b}$$

$$A_j(\omega)=\frac{d_{11}\,\omega^2-n_j^2}{(1+d_{12})\,i\,\omega\,n_j},\quad j=3,4, \tag{9c}$$

$$p_3=-A|\alpha|,\quad p_4=-B|\alpha|, \tag{9d}$$

$$A=\frac{1}{2}\sqrt{\frac{2}{d_{11}}\left(\beta_1+\sqrt{\beta_2}\right)},\quad B=\frac{1}{2}\sqrt{\frac{2}{d_{11}}\left(\beta_1-\sqrt{\beta_2}\right)}, \tag{9e}$$

$$D_j(\alpha)=\frac{\alpha^2-d_{11}p_j^2}{(1+d_{12})\,\alpha\,p_j},\quad j=3,4, \tag{9f}$$

$$\beta_1=d_{11}d_{22}-2d_{12}-d_{12}^2, \tag{9g}$$

$$\beta_2=d_{11}^2d_{22}^2-4d_{11}d_{22}d_{12}-2d_{11}d_{22}d_{12}^2+4d_{12}^2+4d_{12}^3+d_{12}^4-4d_{11}d_{22}. \tag{9h}$$

C_j and B_j, $j=3,4$, in Eq. (8) are unknown functions and determined by using the boundary and continuity conditions. The expressions of these functions are provided in the dissertation by Sarikaya (2014). Note that these unknowns are found in terms of the primary unknown function f_1. n_j and p_j, $j=3,4$, are roots of characteristic equations obtained by applying Fourier transforms to the governing equations. An orthotropic material is classified according to the form of these roots as detailed by Delale and Erdogan (1977). When $\beta_2>0$, $|\beta_1|>\sqrt{\beta_2}$. As a consequence, if $\beta_1>0$ and $\beta_2>0$, all roots are real; and if $\beta_1<0$ and $\beta_2>0$ roots are pure imaginary. The roots are complex if $\beta_2<0$. The orthotropic material is referred to as type I if $\beta_1>0$ and $\beta_2>0$; and as type II if $\beta_2<0$. In the present study, we consider type I orthotropic material, which is commonly encountered in engineering applications such as fiber reinforced composites, and thin films and coatings.

2.1.2. Mode II problem

Mode II problem is formulated in terms of the derivative of the relative tangential crack face displacement. The primary unknown function is expressed in the following form:

$$f_2(x_1) = \frac{C_{66}}{2}\frac{\partial}{\partial x_1}\left(u_1(x_1, 0^+) - u_1(x_1, 0^-)\right), \quad 0 < x_1 < a. \quad (10)$$

The conditions to be satisfied in the formulation of the mode II problem are:

$$\sigma_{11}(0, x_2) = \sigma_{12}(0, x_2) = 0, \quad -\infty < x_2 < \infty, \quad (11a)$$

$$\sigma_{22}(x_1, 0^+) = \sigma_{22}(x_1, 0^-), \quad 0 < x_1 < \infty, \quad (11b)$$

$$\sigma_{12}(x_1, 0^+) = \sigma_{12}(x_1, 0^-), \quad 0 < x_1 < \infty, \quad (11c)$$

$$u_2(x_1, 0^+) = u_2(x_1, 0^-), \quad 0 < x_1 < \infty, \quad (11d)$$

$$u_1(x_1, 0^+) = u_1(x_1, 0^-), \quad a < x_1 < \infty. \quad (11e)$$

Fourier, Fourier cosine, and Fourier sine transforms are applied to find the displacement fields, which are written as follows:

$$u_1(x_1, x_2) = \frac{1}{2\pi}\int_{-\infty}^{\infty}\sum_{j=3}^{4} F_j \exp(n_j x_2 + i\omega x_1)\, d\omega + \int_0^{\infty}\left(\sum_{j=3}^{4} G_j \exp(p_j x_1)\right)\sin(\alpha x_2) d\alpha, \quad x_1 > 0, \quad x_2 > 0, \quad (12a)$$

$$u_2(x_1, x_2) = \frac{1}{2\pi}\int_{-\infty}^{\infty}\sum_{j=3}^{4} F_j A_j \exp(n_j x_2 + i\omega x_1)\, d\omega + \int_0^{\infty}\left(\sum_{j=3}^{4} G_j H_j \exp(p_j x_1)\right)\cos(\alpha x_2) d\alpha, \quad x_1 > 0, \quad x_2 > 0, \quad (12b)$$

where

$$H_j(\alpha) = \frac{d_{11}p_j^2 - \alpha^2}{(1+d_{12})\alpha\, p_j}, \; j = 3, 4. \quad (13)$$

The functions F_j, G_j, $j = 3, 4$, are determined in terms of f_2 by considering boundary and continuity conditions given by Eq. (11); and provided by Sarikaya (2014).

2.2. Contact problem

The contact problem considered is shown in Fig. 3. Primary unknown function in contact formulation is the contact stress at the surface and defined by

$$f_3(x_2) = \sigma_{11}(0, x_2), \quad b < x_2 < c. \quad (14)$$

Boundary conditions read:

$$\sigma_{12}(0, x_2) = \eta\sigma_{11}(0, x_2), \quad b < x_2 < c, \quad (15a)$$

$$\sigma_{11}(0, x_2) = \sigma_{12}(0, x_2) = 0, \quad x_2 < b \text{ and } x_2 > c. \quad (15b)$$

Applying Fourier transform in x_2 to Eqs. (4a) and (4b), displacement components are found to be:

$$u_1(x_1, x_2) = \frac{1}{2\pi}\int_{-\infty}^{\infty}\sum_{j=1}^{2} M_j \exp(s_j x_1 + i\rho x_2)\, d\rho, \quad (16a)$$

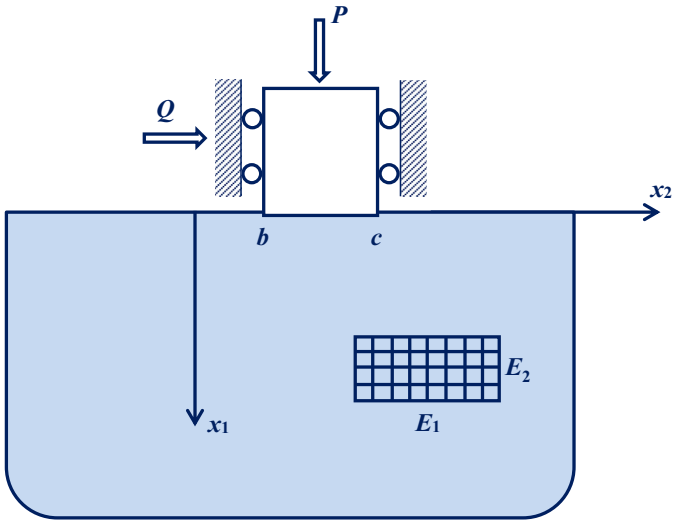

Fig. 3. The contact problem.

$$u_2(x_1, x_2) = \frac{1}{2\pi}\int_{-\infty}^{\infty}\sum_{j=1}^{2} M_j N_j \exp(s_j x_1 + i\rho x_2)\, d\rho, \quad (16b)$$

where,

$$s_1 = -A|\rho|, \quad s_2 = -B|\rho|, \quad (17a)$$

$$N_j(\rho) = \frac{\rho^2 - d_{11}s_j^2}{(1+d_{12})\, i\rho\, s_j}, \quad j = 1, 2. \quad (17b)$$

The unknown functions M_j, $j = 1, 2$, in Eq. (16) are obtained in terms of f_3 by implementing the boundary conditions and written in the form:

$$M_j(\rho) = \frac{2}{C_{66}}\psi_j(\rho)\int_b^c f_3(t)\exp(-i\rho t)\, dt, \; j = 1, 2, \quad (18a)$$

$$\psi_1(\rho) = \frac{\begin{vmatrix} 1 & d_{11}s_2 + d_{12}N_2 i\rho \\ \eta & i\rho + N_2 s_2 \end{vmatrix}}{\Delta_3(\rho)}, \quad \psi_2(\rho) = \frac{\begin{vmatrix} d_{11}s_1 + d_{12}N_1 i\rho & 1 \\ i\rho + N_1 s_1 & \eta \end{vmatrix}}{\Delta_3(\rho)}, \quad (18b)$$

$$\Delta_3(\rho) = \begin{vmatrix} d_{11}s_1 + d_{12}N_1 i\rho & d_{11}s_2 + d_{12}N_2 i\rho \\ i\rho + N_1 s_1 & i\rho + N_2 s_2 \end{vmatrix}. \quad (18c)$$

2.3. Singular integral equations

Displacement field for the coupled crack and contact problem shown in Fig. 1 is obtained by adding up the displacement fields derived for mode I, mode II, and contact problems. Strains and stresses are found by means of kinematic relations and generalized Hooke's law, respectively. The coupled problem is then reduced to a system of three singular integral equations by applying the boundary conditions conveyed by Eq. (5c) and (5d). Derivation procedure of the singular integral equations involves lengthy asymptotic analyses, which are needed to extract the singular terms. These details are not presented here for the sake of brevity but available in the dissertation by Sarikaya (2014). The integral equations are expressed as follows:

$$\sigma_{22}(x_1,0) = \int_0^a \left[\frac{1}{2\pi}\frac{a_{20}}{x_1-t} + h_{11s}(x_1,t) + h_{11f}(x_1,t)\right] f_1(t)\,dt + \int_b^c \left[h_{13s}(x_1,t) + h_{13f}(x_1,t)\right] f_3(t)\,dt = 0, \quad 0 < x_1 < a, \tag{19a}$$

$$\sigma_{12}(x_1,0) = \int_0^a \left[\frac{1}{2\pi}\frac{m_{20}}{x_1-t} + h_{22s}(x_1,t) + h_{22f}(x_1,t)\right] f_2(t)\,dt + \int_b^c \left[h_{23s}(x_1,t) + h_{23f}(x_1,t)\right] f_3(t)\,dt = 0, \quad 0 < x_1 < a, \tag{19b}$$

$$\frac{C_{66}}{2}\frac{\partial}{\partial x_2} u_1(0,x_2) = \int_0^a \left[h_{31s}(x_2,t) + h_{31f}(x_2,t)\right] f_1(t)\,dt + \int_b^c \left[h_{32s}(x_2,t) + h_{31f}(x_2,t)\right] f_2(t)\,dt + \int_b^c \left[\frac{1}{2\pi}\left(\frac{e_{20}}{x_2-t}\right) + \left(\frac{e_{10}}{2}\right)\delta(x_2-t) + h_{33f}(x_2,t)\right] \times f_3(t)\,dt = 0, \quad b < x_2 < c. \tag{19c}$$

$\delta(x_2-t)$ in Eq. (19c) is the Dirac delta function. The constants and functions associated with the integrands are given by Sarikaya (2014).

2.4. Singular behaviors of the unknown functions

Singular behaviors of the primary unknown functions f_1, f_2, and f_3 at the end points of their respective intervals of definition are determined by employing the function-theoretic method, whose details are described by Dag (2001) and Erdogan (1978). The functions may possess power singularities at the ends and thus can be written as

$$f_1(x_1) = x_1^{\theta_1}(a-x_1)^{\lambda_1} F_1(x_1), \quad 0 < x_1 < a, \tag{20a}$$

$$f_2(x_1) = x_1^{\theta_2}(a-x_1)^{\lambda_2} F_2(x_1), \quad 0 < x_1 < a, \tag{20b}$$

$$f_3(x_2) = (x_2-b)^{\omega}(c-x_2)^{\beta} F_3(x_2), \quad b < x_2 < c, \tag{20c}$$

where $F_1(x_1)$, $F_2(x_1)$, and $F_3(x_2)$ are bounded functions; and the exponents θ_1, θ_2, λ_1, λ_2, ω, and β stand for strengths of singularity. Considering these expressions and following the function-theoretic method; the singular integral equations are recast into new forms consisting of dominant terms near the end points. These representations are given by

$$\sigma_{22}(x_1,0) \cong F_1(0)(a)^{\lambda_1}\left\{\frac{a_{20}}{2}\cot(\pi\theta_1) - \frac{\pi}{\sin(\pi\theta_1)} \times \left[b_{110}F(AF)^{\theta_1} + b_{120}E(AE)^{\theta_1} + b_{210}F(BF)^{\theta_1} + b_{220}E(BE)^{\theta_1}\right]\right\} \times (x_1)^{\theta_1} - F_1(a)(a)^{\theta_1}\cot(\pi\lambda_1)(a-x_1)^{\lambda_1} = 0, \quad 0 < x_1 < a, \tag{21a}$$

$$\sigma_{12}(x_1,0) \cong F_2(0)(a)^{\lambda_2}\left\{\frac{m_{20}}{2}\cot(\pi\theta_2) - \frac{\pi}{\sin(\pi\theta_2)} \times \left[n_{110}F(AF)^{\theta_2} + n_{120}E(AE)^{\theta_2} + n_{210}F(BF)^{\theta_2} + n_{220}E(BE)^{\theta_2}\right]\right\} \times (x_1)^{\theta_2} - F_2(a)(a)^{\theta_2}\cot(\pi\lambda_2)(a-x_1)^{\lambda_2} = 0, \quad 0 < x_1 < a, \tag{21b}$$

$$\frac{C_{66}}{2}\frac{\partial}{\partial x_2} u_1(0,x_2) \cong \frac{e_{20}}{2}\left[F_3(b)(c-b)^{\beta}\cot(\pi\omega)(x_2-b)^{\omega} - F_3(c)(c-b)^{\omega}\cot(\pi\beta)(c-x_2)^{\beta}\right] + \frac{e_{10}}{2}F_3(x_2)(x_2-b)^{\omega}(c-x_2)^{\beta} = 0, \quad b < x_2 < c. \tag{21c}$$

The constants A, B, E, and F are given by Eqs. (9b) and (9e); and a_{20}, m_{20}, e_{20}, e_{10}, b_{120}, b_{210}, n_{110}, n_{120}, n_{210}, and n_{220} are available in the dissertation by Sarikaya (2014).

Multiplying Eq. (21a) by $(x_1)^{-\theta_1}$ and letting $x_1 \to 0$, we arrive at the characteristic equation

$$\frac{a_{20}}{2}\cot(\pi\theta_1) - \frac{\pi}{\sin(\pi\theta_1)}[b_{110}F(AF)^{\theta_1} + b_{120}E(AE)^{\theta_1} + b_{210}F(BF)^{\theta_1} + b_{220}E(BE)^{\theta_1}] = 0, \tag{22}$$

and multiplying Eq. (21a) by $(a-x_1)^{-\lambda_1}$ and letting $x_1 \to a$, one finds

$$\cot(\pi\lambda_1) = 0. \tag{23}$$

Eq. (22) has no roots lying in the interval $(-1,0)$ which implies that there is no power singularity for f_1 at $x_1 = 0$. Eq. (23) on the other hand indicates that $\lambda_1 = -0.5$. Operating on Eqs. (21b) and (21c) in a similar way, we derive the characteristic equations

$$\frac{m_{20}}{2}\cot(\pi\theta_2) - \frac{\pi}{\sin(\pi\theta_2)}[n_{110}F(AF)^{\theta_2} + n_{120}E(AE)^{\theta_2} + n_{210}F(BF)^{\theta_2} + n_{220}E(BE)^{\theta_2}] = 0, \tag{24}$$

$$\cot(\pi\lambda_2) = 0, \tag{25}$$

$$\cot(\pi\omega) = -\frac{e_{10}}{e_{20}}, \tag{26}$$

$$\cot(\pi\beta) = \frac{e_{10}}{e_{20}}. \tag{27}$$

Again, Eq. (24) points out that there is no power singularity for f_2 at $x_1 = 0$; and from Eq. (25) it follows that $\lambda_2 = -0.5$. Eqs. (26) and (27) facilitate computation of the strengths of singularity of the unknown function f_3. These exponents depend upon the orthotropic material properties and the coefficient of friction η through e_{10} and e_{20}. Also note that $\omega + \beta = -1$.

3. Numerical solution

In order to be able to numerically solve the singular integral equations, we first define the following substitutions and functions:

$$t = \frac{a}{2}r + \frac{a}{2}, \quad x_1 = \frac{a}{2}s_1 + \frac{a}{2}, \quad -1 < (r,s_1) < 1, \text{ for Eq. (19a)}, \tag{28a}$$

$$t = \frac{a}{2}r + \frac{a}{2}, \quad x_2 = \frac{a}{2}s_2 + \frac{a}{2}, \quad -1 < (r,s_2) < 1, \text{ for Eq. (19b)}, \tag{28b}$$

$$t = \frac{c-b}{2}r + \frac{c+b}{2}, \quad x_3 = \frac{c-b}{2}s_3 + \frac{c+b}{2}, \quad -1 < (r,s_3) < 1, \text{ for Eq. (19c)}, \tag{28c}$$

$$\phi_1(r) = \frac{f_1\left(\frac{a}{2}r + \frac{a}{2}\right)}{P/(c-b)}, \quad -1 < r < 1, \tag{28d}$$

$$\phi_2(r) = \frac{f_2\left(\frac{a}{2}r + \frac{a}{2}\right)}{P/(c-b)}, \quad -1 < r < 1, \tag{28e}$$

$$\phi_3(r) = \frac{f_3\left(\frac{c-b}{2}r + \frac{c+b}{2}\right)}{P/(c-b)}, \quad -1 < r < 1. \tag{28f}$$

The new nondimensional unknown functions are expressed as infinite series involving Jacobi polynomials:

$$\phi_1(r) = (1-r)^{-1/2}\sum_{n=0}^{\infty} A_{1n}P_n^{(-1/2,0)}(r), \quad -1 < r < 1, \tag{29a}$$

$$\phi_2(r) = (1-r)^{-1/2}\sum_{n=0}^{\infty} A_{2n}P_n^{(-1/2,0)}(r), \quad -1 < r < 1, \tag{29b}$$

$$\phi_3(r) = (1-r)^{\beta}(1+r)^{\omega}\sum_{n=0}^{\infty} A_{3n}P_n^{(\beta,\omega)}(r), \quad -1 < r < 1. \tag{29c}$$

A_{in}, $i = 1, \ldots, 3$, here are unknown coefficients of the expansions; and $P_n^{(\beta,\omega)}(r)$ is the Jacobi polynomial of order n. Using $\phi_3 r$ in conjunction with the equilibrium condition given by Eq. (5e), A_{30} is found to be:

$$A_{30} = -\frac{2\Gamma(\beta+\omega+2)}{2^{\beta+\omega+1}\Gamma(\beta+1)\Gamma(\omega+1)}, \tag{30}$$

where Γ is the Gamma function. Substituting Eqs. (29) and (30) into the singular integral equations, regularizing the singular terms, and truncating the infinite series at $n = N$, we reduce the problem to a system of functional linear algebraic equations as given below:

$$\sum_{n=0}^{N} A_{1n}m_{11n}(s_1) + \sum_{n=1}^{N} A_{3n}m_{13n}(s_1) = -A_{30}m_{130}(s_1), \quad -1 < s_1 < 1, \tag{31a}$$

$$\sum_{n=0}^{N} A_{2n}m_{22n}(s_2) + \sum_{n=1}^{N} A_{3n}m_{23n}(s_2) = -A_{30}m_{230}(s_2), \quad -1 < s_2 < 1, \tag{31b}$$

$$\sum_{n=0}^{N} A_{1n}m_{31n}(s_3) + \sum_{n=0}^{N} A_{2n}m_{32n}(s_3) + \sum_{n=1}^{N} A_{3n}m_{33n}(s_3) = -A_{30}m_{330}(s_3), \quad -1 < s_3 < 1. \tag{31c}$$

The functions associated with this system read

$$m_{11n}(s_1) = \frac{a_{20}}{2}\frac{\Gamma(-1/2)\Gamma(n+1)}{\sqrt{2}\pi\,\Gamma(n+1/2)}\mathrm{F}\left(n+1; -n+1/2; 3/2; \frac{1-s_1}{2}\right) + \int_{-1}^{1}(1-r)^{-1/2}P_n^{(-1/2,0)}(r)H_{11}(s_1,r)dr, \tag{32a}$$

$$m_{13n}(s_1) = \int_{-1}^{1}(1-r)^{\beta}(1+r)^{\omega}P_n^{(\beta,\omega)}(r)H_{13}(s_1,r)\,dr, \tag{32b}$$

$$m_{22n}(s_2) = \frac{m_{20}}{2}\frac{\Gamma(-1/2)\Gamma(n+1)}{\sqrt{2}\pi\,\Gamma(n+1/2)}\mathrm{F}\left(n+1; -n+1/2; 3/2; \frac{1-s_2}{2}\right) + \int_{-1}^{1}(1-r)^{-1/2}P_n^{(-1/2,0)}(r)H_{22}(s_2,r)dr, \tag{32c}$$

$$m_{23n}(s_2) = \int_{-1}^{1}(1-r)^{\beta}(1+r)^{\omega}P_n^{(\beta,\omega)}(r)H_{23}(s_2,r)\,dr, \tag{32d}$$

$$m_{31n}(s_3) = \int_{-1}^{1}(1-r)^{-1/2}P_n^{(-1/2,0)}(r)H_{31}(s_3,r)\,dr, \tag{32e}$$

$$m_{32n}(s_3) = \int_{-1}^{1}(1-r)^{-1/2}P_n^{(-1/2,0)}(r)H_{32}(s_3,r)\,dr, \tag{32f}$$

$$m_{33n}(s_3) = \begin{cases} \dfrac{e_{20}}{4}\dfrac{1}{\sin(\pi\beta)}P_{n-1}^{(-\beta,-\omega)}(s_3) + \displaystyle\int_{-1}^{1}(1-r)^{\beta}(1+r)^{\omega} \\ \quad \times P_n^{(\beta,\omega)}(r)H_{33}(s_3,r)\,dr, \ \text{if } n \neq 0, \\ \displaystyle\int_{-1}^{1}(1-r)^{\beta}(1+r)^{\omega}P_n^{(\beta,\omega)}(r)H_{33}(s_3,r)\,dr, \ \text{if } n = 0. \end{cases} \tag{32g}$$

F in Eqs. (32a) and (32c) is the hypergeometric function; and H_{ij} are defined as

$$\begin{aligned} H_{11}(s_1,r) &= \frac{a}{2}\Big(H_{11s}(s_1,r) + H_{11f}(s_1,r)\Big), \\ H_{13}(s_1,r) &= \frac{c-b}{2}\Big(H_{13s}(s_1,r) + H_{13f}(s_1,r)\Big), \end{aligned} \tag{33a}$$

$$\begin{aligned} H_{22}(s_2,r) &= \frac{a}{2}\Big(H_{22s}(s_2,r) + H_{22f}(s_2,r)\Big), \\ H_{23}(s_2,r) &= \frac{c-b}{2}\Big(H_{23s}(s_2,r) + H_{23f}(s_2,r)\Big), \end{aligned} \tag{33b}$$

$$\begin{aligned} H_{31}(s_3,r) &= \frac{a}{2}\Big(H_{31s}(s_3,r) + H_{31f}(s_3,r)\Big), \\ H_{32}(s_3,r) &= \frac{a}{2}\Big(H_{32s}(s_3,r) + H_{32f}(s_3,r)\Big), \end{aligned} \tag{33c}$$

$$H_{33}(s_3,r) = \frac{c-b}{2}H_{33f}(s_3,r), \tag{33d}$$

$$H_{ijs}(s_i,r) = h_{ijs}(x,t), \quad H_{ijf}(s_i,r) = h_{ijf}(x,t), \tag{33e}$$

$$x = \begin{cases} \dfrac{a}{2}s_i + \dfrac{a}{2}, & i = 1, 2, \\ \dfrac{c-b}{2}s_i + \dfrac{c+b}{2}, & i = 3, \end{cases} \qquad t = \begin{cases} \dfrac{a}{2}r + \dfrac{a}{2}, & j = 1, 2, \\ \dfrac{c-b}{2}r + \dfrac{c+b}{2}, & j = 3. \end{cases} \tag{33f}$$

The functional equation system, expressed by Eq. (31), is discretized by means of a collocation scheme. The collocations points, which are selected to be the roots of Chebyshev polynomials of the first kind, are given by:

$$s_{1i} = \cos\left(\frac{\pi(2i-1)}{2(N+1)}\right), \quad s_{2i} = \cos\left(\frac{\pi(2i-1)}{2(N+1)}\right), \quad i = 1, \ldots, N+1, \tag{34a}$$

$$s_{3i} = \cos\left(\frac{\pi(2i-1)}{2N}\right), \quad i = 1, \ldots, N. \tag{34b}$$

Mixed-mode stress intensity factors at the crack tip, and contact stress at the surface can be computed once the unknown coefficients A_{in}, $i = 1, \ldots, 3$, are evaluated. The definitions of the mode I and II stress intensity factors at the crack tip are

$$\begin{aligned} k_1 &= \lim_{x_1 \to a^+}\sqrt{2(x_1-a)}\,\sigma_{22}(x_1,0) \\ &= -\lim_{x_1 \to a^-}\frac{C_{66}}{2}\sqrt{2(a-x_1)}\frac{\partial}{\partial x_1}\Big(u_2(x_1,0^+) - u_2(x_1,0^-)\Big), \end{aligned} \tag{35a}$$

$$\begin{aligned} k_2 &= \lim_{x_1 \to a^+}\sqrt{2(x_1-a)}\,\sigma_{12}(x_1,0) \\ &= -\lim_{x_1 \to a^-}\frac{C_{66}}{2}\sqrt{2(a-x_1)}\frac{\partial}{\partial x_1}\Big(u_1(x_1,0^+) - u_1(x_1,0^-)\Big). \end{aligned} \tag{35b}$$

Through the use of these definitions and Eq. (29), normalized SIFs are expressed as

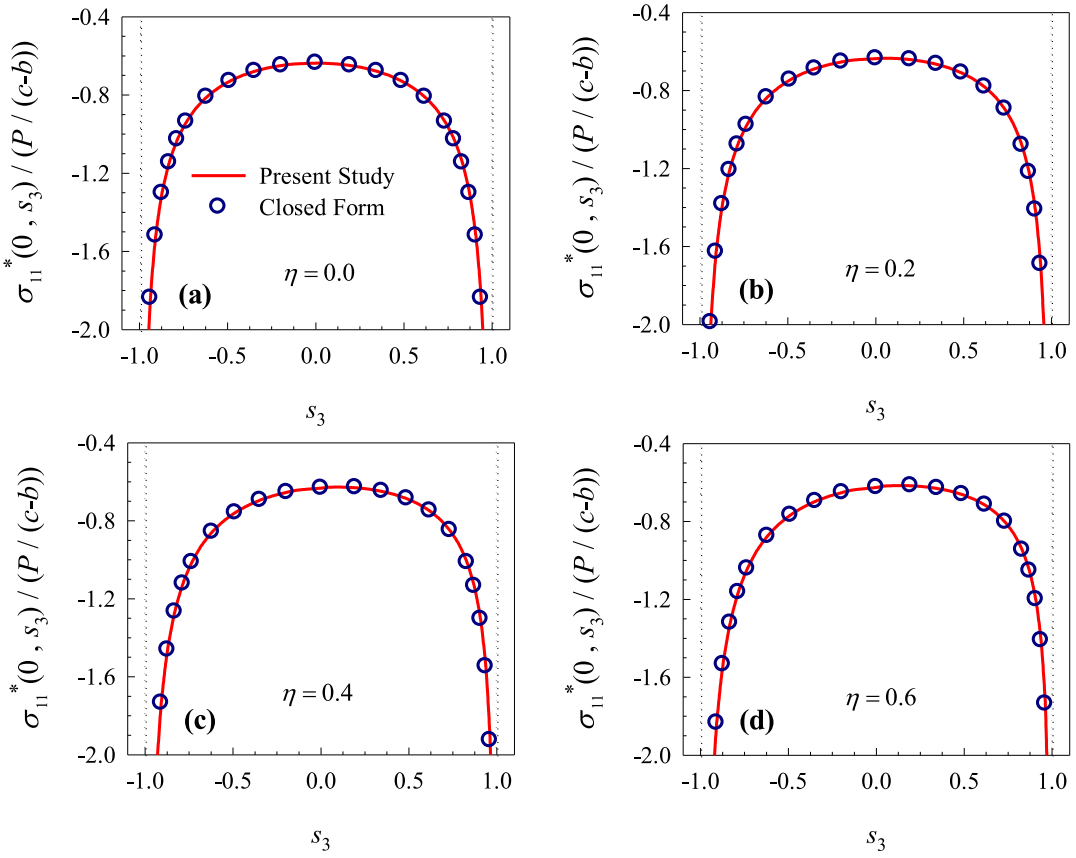

Fig. 4. Comparisons of the computed normalized contact stress to the closed form solution for an orthotropic half-plane: (a) $\eta = 0.0$; (b) $\eta = 0.2$; (c) $\eta = 0.4$; (d) $\eta = 0.6$, $(c-b)/a = 1.0, b/a = 6$.

$$\frac{k_1\sqrt{a}}{P} = k_{1n} = -\frac{a}{c-b}\sum_{n=0}^{N} A_{1n}\, P_n^{(-1/2,\,0)}(1),\ \frac{k_2\sqrt{a}}{P} = k_{2n} = -\frac{a}{c-b}\sum_{n=0}^{N} A_{2n}\, P_n^{(-1/2,\,0)}(1). \tag{36}$$

Normalized contact stress on the other hand is of the form:

$$\frac{\sigma_{11}\left(0,\ \frac{c-b}{2}s_3 + \frac{c+b}{2}\right)}{P/(c-b)} = \frac{\sigma_{11}^{*}(0,s_3)}{P/(c-b)} = (1-s_3)^{\beta}(1+s_3)^{\omega} \times \sum_{n=0}^{N} A_{3n}\, P_n^{(\beta,\omega)}(s_3),\ -1 < s_3 < 1. \tag{37}$$

4. Numerical results

In parametric analyses, normalized stress intensity factors and contact stresses described by Eqs. (36) and (37) are computed as functions of orthotropic material properties, coefficient of friction, and normalized dimensions. To be able to verify the formulation and developed solution procedures, we made comparisons to the results available in the technical literature for certain special cases. The first set of comparisons is provided in Fig. 4, in which normalized contact stresses are compared to the results obtained by using the closed form contact mechanics solution formulated by Galin (Kachanov et al., 2003). This solution is for an orthotropic half-plane in frictional contact with a rigid flat punch; and does not take cracking into account. As a sample orthotropic material, plasma-sprayed alumina is considered in the computations. The elastic properties of orthotropic alumina are given as follows (Dag, 2006):

$$E_1 = 116.36\ \text{GPa},\quad E_2 = 90.43\ \text{GPa},\quad \mu_{12} = 38.21\ \text{GPa}, \tag{38a}$$

$$\nu_{12} = 0.28,\quad \nu_{13} = 0.27,\ \nu_{31} = 0.21,\quad \nu_{32} = 0.14. \tag{38b}$$

Once these values are provided, remaining elastic properties ν_{21}, ν_{23}, and E_3 can be found employing the relations

$$\frac{\nu_{12}}{E_1} = \frac{\nu_{21}}{E_2},\quad \frac{\nu_{13}}{E_1} = \frac{\nu_{31}}{E_3},\quad \frac{\nu_{23}}{E_2} = \frac{\nu_{32}}{E_3}, \tag{39}$$

The results presented in Fig. 4 are generated by setting $(c-b)/a$ and b/a as 1.0 and 6.0, respectively. $(c-b)/a$ is the ratio of the contact zone size to the crack length; and b/a represents relative punch location. Normalized contact stresses are plotted with respect to the nondimensional coordinate s_3 defined by Eq. (28c). A relatively larger value is assigned to b/a to be able to suppress the influence of the crack on the contact stress distribution. It can be seen that for each of the four different friction coefficients considered, our results are in excellent agreement with those obtained through Galin's solution.

The second set of comparisons provided in Fig. 5 involves normalized mode I and II stress intensity factors for a surface crack in an isotropic half-plane, that is loaded by a rigid flat punch. The results produced by the method described in Section 3 are compared to those given by Dag (2001). The figure shows normalized mixed-mode stress intensity factors k_{1n} and k_{2n} as functions of relative punch location b/a and friction coefficient η. The ratio of the contact zone size to crack length $(c-b)/a$ is taken as 1.0. Our results are in very good agreement with those computed by Dag (2001), which is indicative of the high degree of accuracy attained by the application of the methods developed in the present study.

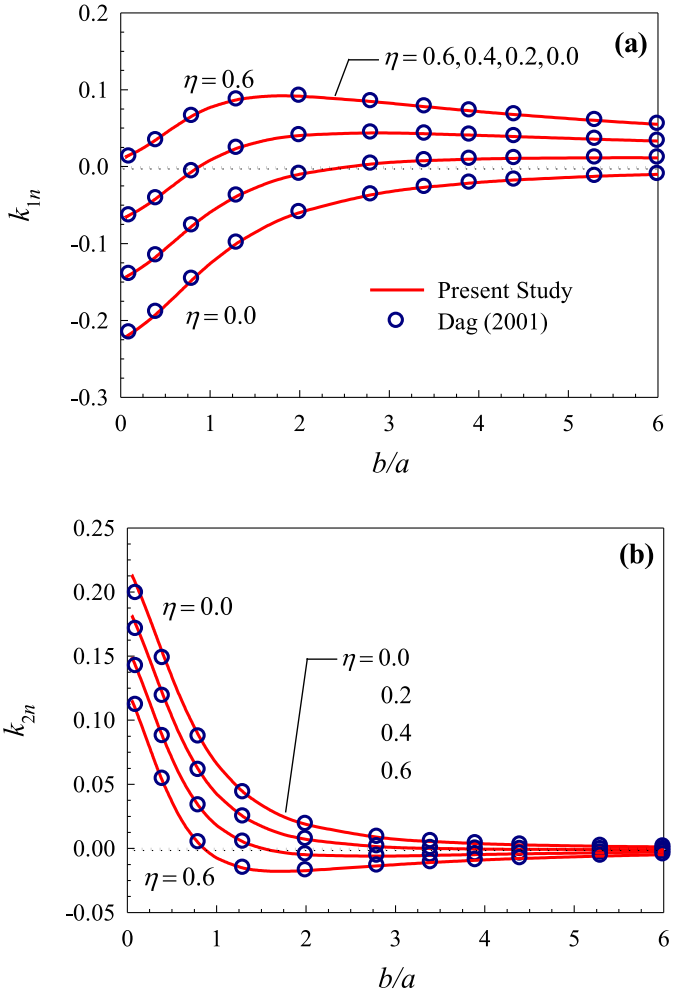

Fig. 5. Comparisons of the normalized mode I and II stress intensity factors for an isotropic half-plane: (a) mode I SIFs; (b) mode II SIFs. $(c-b)/a = 1.0, \nu_{12} = \nu_{13} = \nu_{31} = \nu_{32} = 0.25$.

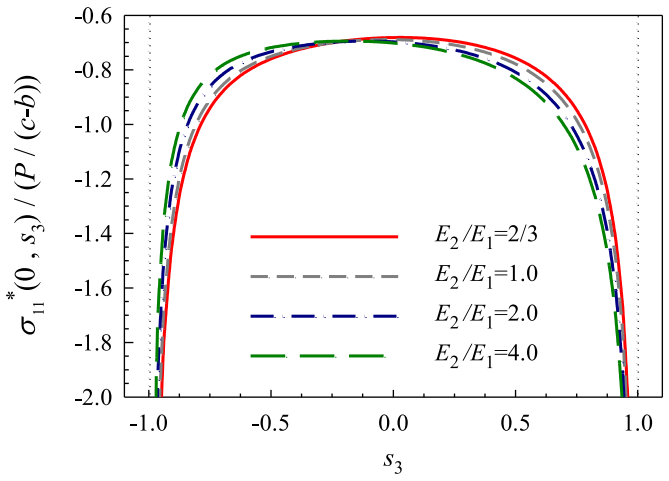

Fig. 6. Normalized contact stress distributions for different values of the modulus ratio E_2/E_1, $(c-b)/a = 1.0, b/a = 0.1, \eta = 0.4$.

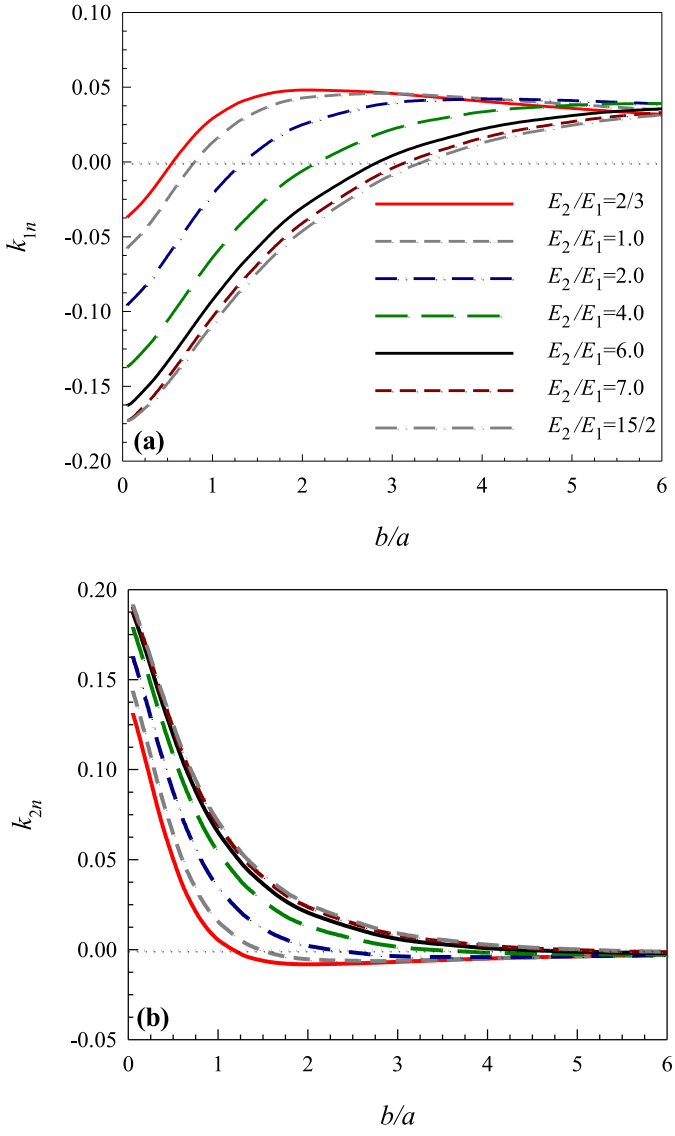

Fig. 7. Normalized mixed-mode stress intensity factors as functions of b/a and the modulus ratio E_2/E_1: (a) mode I SIFs; (b) mode II SIFs. $(c-b)/a = 1.0, \eta = 0.4$.

The new results calculated for the coupled problem depicted by Fig. 1 are provided in Figs. 6–12. In Figs. 6 and 7, we display the influence of the variation in the elastic modulus E_2 upon the contact stress and the mixed-mode stress intensity factors, respectively. In the generation of this group of results, the base material considered is plasma-sprayed alumina, whose properties are given by Eq. (38). All properties given in this equation are kept constant except for the elastic modulus E_2, which is varied to be able to examine the influence of orthotropy. The degree of orthotropy is quantified by the ratio E_2/E_1. Fig. 6 shows the effect of the change in E_2 on the normalized contact stress. It is seen that as E_2/E_1 increases, stress magnitude decreases slightly near the trailing end of the contact zone, and increases near the leading end. The influence of the change in E_2/E_1 is rather pronounced on the normalized mixed-mode stress intensity factors k_{1n} and k_{2n} as evidenced by Fig. 7. The results provided in this figure are generated by considering a wider range of E_2/E_1 including larger values. Note that E_2/E_1 cannot be increased arbitrarily due to the constraints conveyed by Eq. (3). With the orthotropy constants specified by Eq. (38), largest possible E_2/E_1 is 7.5. When the punch is closer to the crack plane, i.e. when b/a is relatively small, normalized mode I SIF decreases and normalized mode II SIF increases with a corresponding rise in E_2. Higher degree of negativity in the mode I SIF for larger E_2/E_1 implies more extensive crack closure for these values of the modulus ratio. As b/a is increased further, mode II SIF

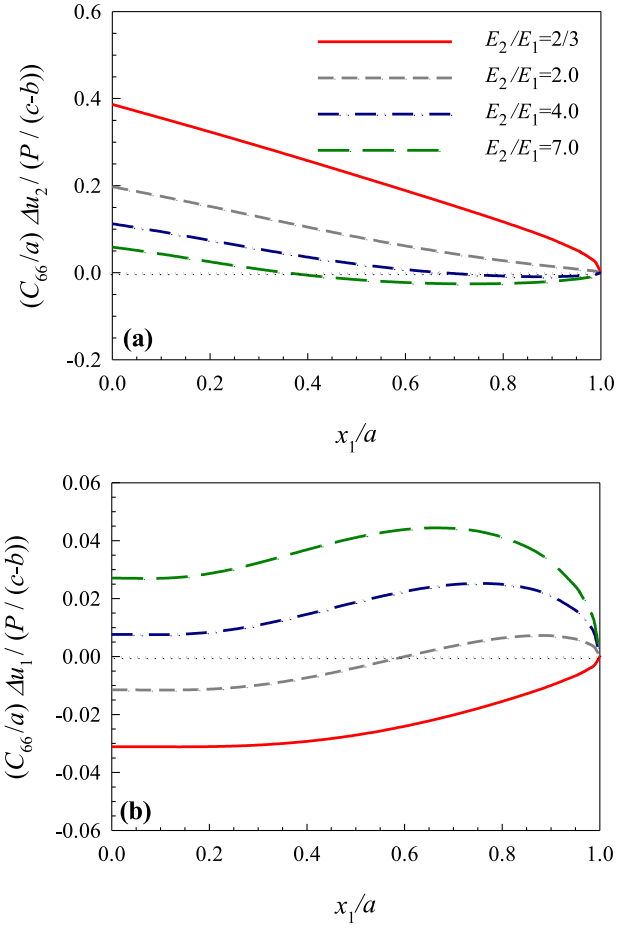

Fig. 8. Normalized relative crack face displacement distributions for various values of the modulus ratio E_2/E_1: (a) normal relative displacements; (b) tangential relative displacements. $(c-b)/a = 1.0, \eta = 0.4, b/a = 1.6$.

rapidly levels off around zero whereas mode I SIF exhibits a more gradual drop in magnitude.

Fig. 8 shows normalized relative crack opening displacements for various values of the modulus ratio E_2/E_1. Normalized relative displacements are found by integrating Eqs. (6) and (10), and given by

$$\frac{C_{66}}{a}\frac{\Delta u_2(x_1)}{P/(c-b)} = \left(\frac{x_1}{a}-1\right)\int_{-1}^{1}\phi_1\left(\frac{x_1}{a}r - r + \frac{x_1}{a}\right)dr, \quad \Delta u_2(x_1) = u_2\left(x_1,0^+\right) - u_2\left(x_1,0^-\right), \quad 0 < x_1 < a, \tag{40a}$$

$$\frac{C_{66}}{a}\frac{\Delta u_1(x_1)}{P/(c-b)} = \left(\frac{x_1}{a}-1\right)\int_{-1}^{1}\phi_2\left(\frac{x_1}{a}r - r + \frac{x_1}{a}\right)dr, \quad \Delta u_1(x_1) = u_1\left(x_1,0^+\right) - u_1\left(x_1,0^-\right), \quad 0 < x_1 < a. \tag{40b}$$

For $E_2/E_1 = 2/3$, k_{1n} is positive, crack is open, and relative normal displacement Δ_2 is seen to be positive for all values of x_1/a. Relative tangential displacement Δ_1 on the other hand is negative for this value of modulus ratio. As E_2/E_1 is increased, crack closure occurs and relative normal displacement becomes negative near the crack tip. Relative tangential displacement continually increases with the corresponding rise in E_2/E_1. Increase in the size of the contact zone is manifested by the extension of the region where Δ_1 is negative. But, calculation of the exact contact zone size requires specification of the contact conditions in the formulation and implementation of an iterative procedure.

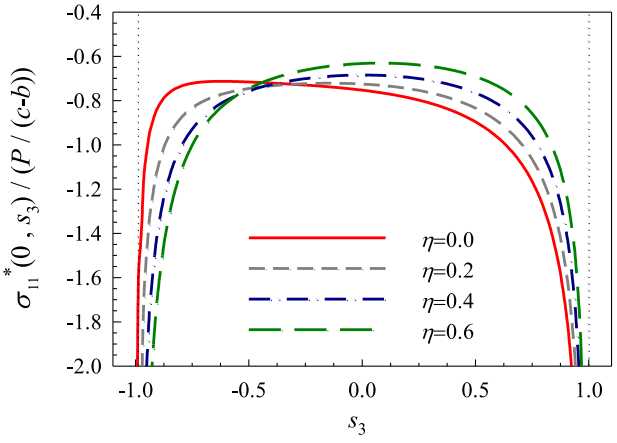

Fig. 9. Normalized contact stress distributions for different values of the friction coefficient η, $(c-b)/a = 1.0, b/a = 0.1$.

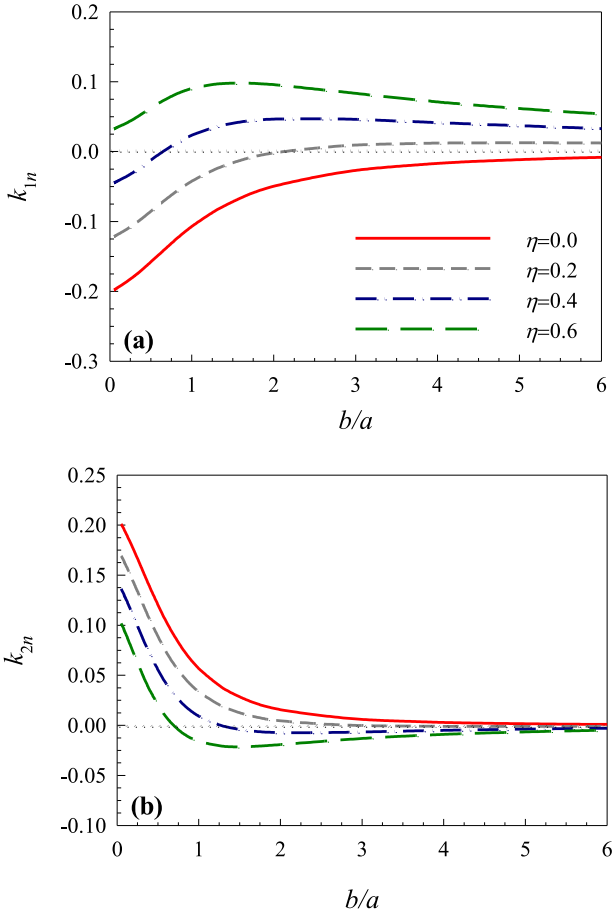

Fig. 10. Normalized mixed-mode stress intensity factors as functions of b/a and the friction coefficient η: (a) mode I SIFs; (b) mode II SIFs. $(c-b)/a = 1.0$.

Figs. 9 and 10 illustrate the effect of the coefficient of friction η on the contact stress and the mixed-mode stress intensity factors for an orthotropic medium. Plasma sprayed orthotropic alumina is the half-plane material. When $\eta = 0$, the contact stress curve slants towards the trailing end of contact, i.e. towards $s_3 = -1$. The curve shifts towards the leading end as the friction coefficient gets larger. The influence upon both of the stress intensity factors is notable. For frictionless contact, mode I SIF is negative whereas mode II SIF is positive. Negativity of the mode I stress intensity factor implies crack closure. As η is increased, mode I SIF also increases and

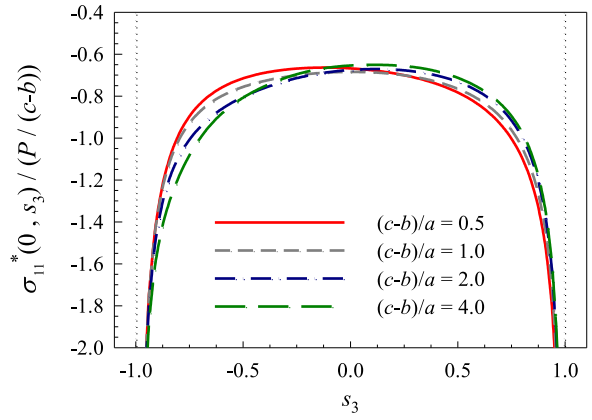

Fig. 11. Normalized contact stress distributions for different values of the contact zone size to crack length ratio $(c-b)/a, \eta = 0.4, b/a = 0.1$.

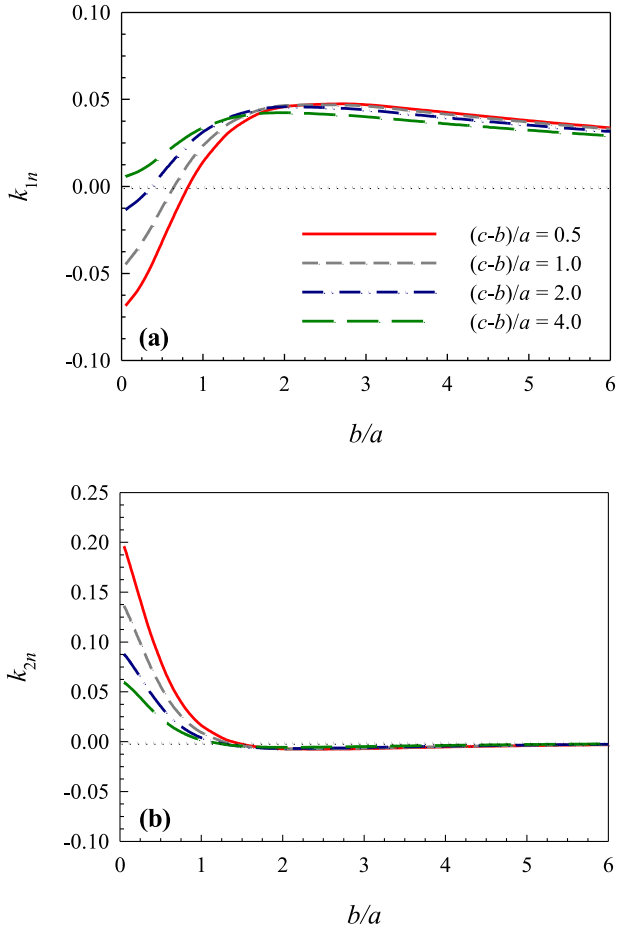

Fig. 12. Normalized mixed-mode stress intensity factors as functions of b/a and contact zone size to crack length ratio $(c-b)/a$: (a) mode I SIFs; (b) mode II SIFs. $\eta = 0.4$.

becomes completely positive for $\eta = 0.6$. Mode II SIF is smaller for larger friction coefficients; and assumes negative values for certain combinations of η and b/a. A reversal in the sign of k_{2n} points to a deviation in the path of crack propagation.

In Figs. 11 and 12, we present contact stress and mode I and II stress intensity factors as functions of contact zone size to crack length ratio $(c-b)/a$ and relative stamp location b/a. The base material is again plasma sprayed alumina. The variation in $(c-b)/a$ is seen to lead to a slight change in the contact stress magnitude. This change is in the form a magnitude rise near the trailing end and a magnitude drop near the leading end for increasing $(c-b)/a$. The influence upon the mixed-mode SIFs is significant for relatively small values of b/a. Within this zone, an increase in $(c-b)/a$ results in a larger mode I SIF and a smaller mode II SIF.

5. Summary and final remarks

This study puts forward an analytical method, which is capable of tackling the coupled surface crack and contact problem in an elastic orthotropic medium. The general solution for the coupled problem is constructed by superposing the separate solutions obtained for opening and sliding mode crack problems; and contact problem. A system of three coupled singular integral equations is then derived utilizing crack surface and contact zone conditions. The system is solved numerically by means of an expansion–collocation technique. Comparisons to the closed-form contact solution of Galin (Kachanov et al., 2003) and the mixed-mode stress intensity factors provided by Dag (2001) demonstrate the high level of accuracy of the results generated through the proposed procedures. Further numerical results are presented to illustrate the dependences of fracture behavior and contact stress on material and geometric properties, and friction coefficient.

It is shown that each of the parameters modulus ratio, coefficient of friction, and contact zone size to crack length ratio has a notable effect on the mode I and II stress intensity factors. For certain combinations of these quantities, the mode I stress intensity factor turns out to be negative, which indicates crack closure. Yet, the results generated in the case of closure will still be applicable if they are employed in a superposition procedure for a combined loading that results in a completely open crack. Contact of crack faces is treated by implementing a different type of procedure. Because of the nonlinearity stemming from the unknown size of the contact zone, this procedure is iterative. Additionally, contact condition needs to be imposed for the crack-contact region. Although crack face contact is not within the scope of the current study, its consideration as future work will provide valuable information regarding fracture behavior especially for small friction coefficients.

The effects of the problem parameters upon the mixed-mode SIFs are pronounced especially when the rigid punch is in close proximity of the crack plane, i.e. when b/a is small. A small b/a value implies a higher degree of coupling between crack and contact problems. The method introduced in this article is perfectly suitable for such configurations since crack-contact coupling is fully taken into consideration. Thus, the analytical solution procedures presented are expected to prove useful in developing a better insight into critical and subcritical crack propagation phenomena in orthotropic media subjected to contact loading.

References

Agarwal, B.D., Broutman, L.J., 1990. Analysis and Performance of Fiber Composites. John Wiley and Sons, Inc, New York.
Baghestani, A.M., Fotuhi, A.R., Fariborz, S.J., 2013. Multiple interacting cracks in an orthotropic layer. Arch. Appl. Mech. 83, 1549–1567.
Dag, S., 2001. Crack and contact problems in graded materials. Ph.D. Dissertation, Lehigh University. Bethlehem PA, USA.
Dag, S., Erdogan, F., 2002. A surface crack in a graded medium loaded by a sliding rigid stamp. Eng. Fract. Mech. 69, 1729–1751.
Dag, S., 2006. Thermal fracture analysis of orthotropic functionally graded materials using an equivalent domain integral approach. Eng. Fract. Mech. 73, 2802–2828.
Delale, F., Erdogan, F., 1977. The problem of internal and edge cracks in an orthotropic strip. J. Appl. Mech. - T. ASME 44, 237–242.
Dong, X.-Q., Zhou, Y.-T., Wang, L.-M., Ding, S.-H., Park, J.-B., 2014. Stress state of two collinear stamps over the surface of orthotropic materials. Arch. Appl. Mech. 84, 639–656.
Erdogan, F., 1978. Mixed Boundary Value Problems in Mechanics. In: Nemat–Nasser, S. (Ed.). Mechanics Today, vol. 4. Pergamon Press, New York.
Hasebe, N., Okumura, M., Nakamura, T., 1989. Frictional punch and crack in plane elasticity. J. Eng. Mech. - ASCE 115, 1137–1149.

Hasebe, N., Qian, J., 1998. Edge crack due to rigid punch in incomplete contact. Mech. Mater. 28, 271–279.
Hills, D.A., Nowell, D., 2014. Mechanics of fretting fatigue–Oxford's contribution. Tribol. Int. 76, 1–5.
Kachanov, M., Shafiro, B., Tsukrov, I., 2003. Handbook of Elasticity Solutions. Kluwer Academic Publishers, Dordrecht.
Lawn, B., 1995. Fracture of Brittle Solids. Cambridge University Press, Cambridge.
Matbuly, M.S., Nassar, M., 2003. Elastostatic analysis of edge cracked orthotropic strips. Acta Mech 165, 17–25.
Monfared, M.M., Ayatollahi, M., 2012. Elastodynamic analysis of a cracked orthotropic half-plane. Appl. Math. Model. 36, 2350–2359.
Nesladek, M., Spaniel, M., Jurenka, J., Ruzicka, J., Kuzelka, J., 2012. Fretting fatigue - Experimental and numerical approaches. Int. J. Fatigue 44, 61–73.
Nobile, L., Piva, A., Viola, E., 2004. On the inclined crack problem in an orthotropic medium under biaxial loading. Eng. Fract. Mech. 71, 529–546.
Page, T.F., Knight, J.C., 1989. Factors affecting the tribological behaviour of thin hard TiN and TiC coatings. Surf. Coat. Tech. 39–40, 339–354.
Sarikaya, D., 2014. A surface crack in an orthotropic medium subjected to sliding contact by a rigid stamp. Ph.D. Dissertation, Middle East Technical University. Ankara, Turkey.
Shi, D., Lin, Y., Ovaert, T.C., 2003. Indentation of an orthotropic half-space by a rigid ellipsoidal indenter. J. Tribol.-T. ASME 125, 223–231.
Suresh, S., Olsson, M., Giannakopoulos, A.E., Padture, N.P., Jitcharoen, J., 1999. Engineering the resistance to sliding-contact damage through controlled gradients in elastic properties at contact surfaces. Acta Mater 47, 3915–3926.
Swanson, S.R., 2004. Hertzian contact of orthotropic materials. Int. J. Solids Struct. 41, 1945–1959.
Zhong, X.C., Wu, B., Zhang, K.-S., 2013. Thermally conducting collinear cracks engulfed by thermomechanical field in a material with orthotropy. Theor. Appl. Fract. Mech. 65, 61–68.
Zhou, Y.T., Lee, K.Y., Jang, Y.H., 2014. Indentation theory on orthotropic materials subjected to a frictional moving punch. Arch. Mech. 66, 71–94.